[William Roberts, Hao He, Jian Li, and Petre Stoica]

Probing Waveform Synthesis and Receiver Filter Design

[A review of recent novel, cyclic approaches to single and multiple waveform designs]

Probing waveform synthesis and receive filter design play crucial roles in achievable performance for many active sensing applications, including radar, sonar, medical imaging, and communications (channel estimation and spread spectrum). A flexible receive filter design approach can be used to compensate for missing features of the probing waveforms, at the costs of lower signal-to-noise ratio (SNR) and higher computational complexity. A well-synthesized waveform, meaning one with good auto- and cross-correlation properties, can reduce computational burden at the receiver and improve performance. In this article, we will highlight the interplay between waveform synthesis and receiver design. We will provide a tutorial review of recent novel, cyclic approaches to single and multiple waveform designs. Both aperiodic and periodic correlations will be considered. We show that by making use of fast Fourier transforms (FFTs), we can now efficiently design sequences that were previously impossible to synthesize. Furthermore, we will provide an overview of some advanced techniques for receiver design, including data-independent instrumental variables (IV) filters and a data-adaptive iterative approach. We will show how these designs can significantly outperform conventional techniques in various active sensing applications.

INTRODUCTION

Areas of active sensing (including radar, sonar, medical imaging, and communications) have garnered the attention of researchers for decades. The goal of any active sensing application is the transmission and reception of one or more chosen waveforms. A received signal may be analyzed to determine properties of a propagation medium, as in channel estimation for communications, or to estimate the location and strength of targets in a scene, as in medical imaging for breast cancer detection.

Digital Object Identifier 10.1109/MSP.2010.936724

Performance, in a most general sense, is measured simply by the accuracy with which an interpretation of the received signal matches the true information in the scene.

Not surprisingly, a system's performance is linked directly to the behavior of its transmitted waveform(s), which has resulted in a vast amount of literature devoted to the study of sequence design (e.g., see [1]–[4]). The foundation of research in signal transmission has been built, over the last century, on work from such notable theorists as Shannon, Nyquist, and Tesla. Following World War II, the development and characterization of transmission sequences was furthered by such researchers as Woodward, Barker, Frank, and Golomb. Waveform synthesis remains a dynamic research area even in modern times, as continued improvements in waveform generation and receiving hardware allow for increasingly advanced sequence design. As computational limitations on waveform design and transmission are relaxed, new approaches and improved performance become possible.

In this article, we will offer a tutorial description of some of the very latest algorithms for sequence design. Our discussion is an extension to the recent special issue [5], which focused on several new strategies for waveform development in radar systems. In [6], a design scheme for periodic constant amplitude with zero autocorrelation (CAZAC) sequences is presented for single waveform transmissions. Another article [7] in the special issue explores the design of complementary sequences. Herein, we focus primarily on waveforms with good aperiodic correlations, and we show that our designs can be extended to design periodic CAZAC sequences as well. We consider both single sequence and multiple sequence set designs. The design of multiple sequences with good auto- and cross-correlation properties is demanded in the emerging fields of multiple-input, multiple-output (MIMO) radar and MIMO communications (see, e.g., [8]–[11]). Further, since our goal is improved system performance, we will give an overview of several novel receiver design techniques. We will clearly illustrate how receiver design can be used to compensate for deficiencies in waveform synthesis.

THE ACTIVE SENSING PROBLEM

Consider the synthesis of a single sequence with good aperiodic autocorrelation, which is widely needed in conventional single-input, single-output (SISO) radar, sonar, and medical imaging applications. In SISO radar, for example, a pulse is transmitted in the direction of a scene of interest [12]. The signal is reflected by targets in the scene, which could be at different angular and range locations relative to the radar. The reflected signals, which are attenuated and time-shifted versions of the transmitted waveform, are linearly combined at the receive antenna (which could be the same as or different from the one used for transmission). Signal processing of the received signal is performed to determine unknown properties of the targets, such as their range, radar cross section (RCS), and speed (or Doppler shift).

We let $s(t)$ denote a transmitted waveform of duration τ and comprising N subpulses (so that each subpulse has a duration of τ/N). We can then represent $s(t)$ by the vector $\mathbf{x}$, whose components correspond to the phase-coded amplitude of each subpulse (we assume rectangular subpulses)

$$\mathbf{x} = [x(1), \quad x(2), \quad \ldots, \quad x(N)]^T, \tag{1}$$

where $(\cdot)^T$ denotes the transpose operation. Due to hardware constraints (such as the limitations of the power amplifier) in practice, components of the transmitted waveform are commonly restricted to being constant modulus. Without loss of generality, we consider $\{x(n)\}_{n=1}^{N}$ being unimodular, so that

$$x(n) = e^{j\phi_n}, \ \ n = 1, \ \ldots, N, \tag{2}$$

where ϕ_n represents the phase of $x(n)$. If the set of targets in the scene are represented by their RCSs $\{\kappa_{r,l}\}$ (for $r = 1, \ldots, R$ denoting the range bin and $l = 1, \ldots, L$ denoting the Doppler bin of a target), then the received signal $\mathbf{y}_{r'}$ (aligned with the transmitted waveform's reflection from a range bin of interest r') can be modeled as

$$\mathbf{y}_{r'} = \kappa_{r',l'}\widetilde{\mathbf{x}}_{l'} + \sum_{\substack{n=-N+1 \\ (r'+n,l)\neq(r',l')}}^{N-1} \sum_{l=1}^{L} \kappa_{r'+n,l}\, \mathbf{J}_n \widetilde{\mathbf{x}}_l + \boldsymbol{\varepsilon}, \tag{3}$$

where $\kappa_{r',l'}$ refers to the reflection coefficient of a target of interest and $\boldsymbol{\varepsilon}$ refers to the noise component of the received signal. Further, $\mathbf{J}_n$ is a shift matrix designed to temporally align the reflected signal from a target that lies n range bins away from the bin of interest

$$\mathbf{J}_n = \begin{bmatrix} 0 & & & 0 \\ \vdots & & & \\ 1 & & & \\ & 1 & & \\ & & \ddots & \\ 0 & & \underbrace{1 \cdots 0}_{n+1} & \end{bmatrix}_{N\times N} = \mathbf{J}_{-n}^T, \quad n = 0, 1, \ldots, N-1. \tag{4}$$

We assume that, in general, $\kappa_{r,l} = 0$ for any r such that $r \notin \{1, \ldots, R\}$. We let $\widetilde{\mathbf{x}}_l = \mathbf{x} \odot \mathbf{a}_l$ denote the Doppler shifted waveform ($\odot$ refers to the Hadamard product operation), and

$$\mathbf{a}_l = [1, \ \ e^{j\omega_l}, \quad \ldots, \ \ e^{j\omega_l(N-1)}]^T, \ \ l = 1, \ldots, L, \tag{5}$$

where ω_l represents the Doppler frequency for the lth Doppler bin (we assume L bins divide the Doppler interval of interest). We illustrate the model for $\mathbf{y}_{r'}$ in Figure 1 (the Doppler effect is not shown). The problem of interest for this SISO radar case, as well as for any other active sensing application, is the successful estimation of the unknown target coefficients given by $\{\kappa_{r,l}\}$.

TRANSMIT WAVEFORM DESIGN

Neglecting interferences from other range bins, which are represented by the clutter returns in Figure 1, a matched filter can be used to provide optimal performance (the highest SNR) in

the presence of stochastic additive white noise. When clutter affects the received signal, a matched filter will function optimally only if the autocorrelation sidelobe terms of the transmit waveform, given by

$$r(\Delta t) \triangleq \int s(t)s^*(t-\Delta t)dt, \quad \forall \Delta t \neq 0 \tag{6}$$

are zero, where $(\cdot)^*$ denotes the complex conjugate for scalars and the conjugate transpose operation for vectors and matrices.

For most modern sensing systems, filtering at the receiver is performed digitally. Further, when rectangular subpulses are adopted at the transmitter, values of $r(\Delta t)$ can be obtained exactly by a linear combination of two neighboring correlations evaluated at integer multiples of τ/N (approximations can be made when nonrectangular shaping pulses are used) [3]. Thus, in most practical cases, we can restrict our attention to the autocorrelation of the discrete sequence $\{x(n)\}_{n=1}^N$

$$r_k = \sum_{n=k+1}^{N} x(n)x^*(n-k) = r_{-k}^*, \quad k = 0, \ldots, N-1. \tag{7}$$

No signal in practice can have zero sidelobes for all $k \neq 0$ in (7) (since, e.g., $|r_{N-1}| = |r_{-N+1}| = 1$ for all unimodular sequences). Therefore, a legitimate goal in transmit sequence design would be to construct $\{x(n)\}_{n=1}^N$ such that the autocorrelation sidelobes $\{r_k, (k \neq 0)\}$ are as small as possible. In other words, waveforms with high merit factors (MFs) are desirable [13], [14], where we let

$$\text{MF} = \frac{N^2}{\text{ISL}}, \tag{8}$$

with

$$\text{ISL} = \sum_{\substack{k=-(N-1) \\ k\neq 0}}^{N-1} |r_k|^2. \tag{9}$$

ISL refers to the integrated sidelobe level of the autocorrelation function. In the next subsection, we will review several existing waveforms (including several phase-coded waveforms) that have good autocorrelation properties.

A REVIEW OF EXISTING WAVEFORMS

In 1953, Barker introduced a set of binary codes (meaning $\phi_n \in \{-\pi, \pi\}$ for $n = 1, \ldots, N$) that yield a peak-to-peak sidelobe ratio of N and subsequently the highest MF for binary sequences of equal length [15]. However, the longest known Barker sequence is of length 13, and researchers contend that no longer waveforms can satisfy the Barker criteria [3], [16], [17]. To identify binary sequences that yield a maximum MF (for a given N) requires an exhaustive search whose computational complexity increases exponentially with the length, which quickly proves intractable as N increases. At the cost of increased hardware complexity, the binary restriction can be relaxed to design unimodular sequences (which may or may not use a finite alphabet) with lower sidelobe levels and higher merit factors.

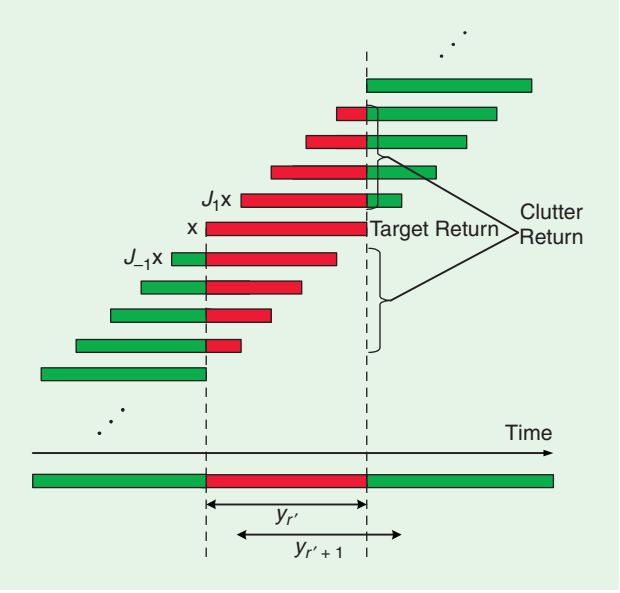

[FIG1] Received signal aligned with the return from a target in range bin r'.

Many well-known unimodular phase-coded signals are derived from the phase history of a chirp waveform. A chirp is a linear frequency-modulated (LFM) pulse whose frequency is swept linearly over a bandwidth B in the sequence's time duration τ. Chirp waveforms have been widely used for radar applications since World War II, as they possess relatively low peak sidelobe levels and are mostly tolerant to shifts in Doppler frequency [3]. In addition, chirp signals have spectral efficiency, meaning the power of the waveforms is dispersed evenly throughout the frequency spectrum, which allows for high range resolution.

The chirp waveform $s(t)$ is given by

$$s(t) = \frac{1}{\sqrt{\tau}} e^{j\pi\frac{B}{\tau}t^2}, \quad 0 \le t \le \tau, \tag{10}$$

where B/τ is the chirp rate of the signal. By sampling $s(t)$ at time intervals $t_s(n) = n/B$, for $n = 1, \ldots, N$ $(N = BT)$, and by omitting the multiplicative term $1/\sqrt{\tau}$, the following discrete sequence is obtained:

$$\begin{aligned} x(n) &= s(t_s(n)) = e^{j\pi\frac{B}{\tau}\left(\frac{n}{B}\right)^2} \\ &= e^{j\pi\frac{n^2}{BT}} = e^{j\pi\frac{n^2}{N}}, \quad n = 1, \ldots, N. \end{aligned} \tag{11}$$

The signal $\{x(n)\}_{n=1}^N$ shown in (11) has perfect periodic autocorrelation if N is even, meaning that all periodic autocorrelation sidelobes are zero

$$\tilde{r}(k) = \sum_{n=1}^{N} x(n)x^*((n+k) \bmod N) = 0, \quad 1 \le k \le N-1, \tag{12}$$

where $(a \bmod b) = a - \lfloor a/b \rfloor b$. We refer to waveforms with perfect periodic autocorrelations as CAZAC sequences, which were

thoroughly reviewed in [6]. A set of CAZAC sequences can also be constructed, for odd values of N, by altering (11) as follows:

$$x(n) = e^{j\pi\frac{n(n-1)}{N}}, \quad n = 1, \ldots, N, \tag{13}$$

which is the famous Golomb sequence [18].

The Frank code [19], which was first presented in 1963, is perhaps the most well-known CAZAC sequence. Frank signals are also derived from the phase history of a chirp waveform, and are defined for a square $N = K^2$ length sequence as

$$x((m-1)K + p) = e^{j2\pi\frac{(m-1)(p-1)}{K}}, \quad m, p = 1, \ldots, K. \tag{14}$$

Similarly, P4 sequences [20] are phase-coded CAZAC waveforms whose phases are quadratic functions of n. The P4 sequence is defined for any length N as

$$x(n) = e^{j\frac{2\pi}{N}(n-1)\left(\frac{n-1-N}{2}\right)}, \quad n = 1, \ldots, N. \tag{15}$$

CAZAC sequences, both chirp like and nonchirp like, have been shown to exist for any length N [6] (infinite number of sequences exist for some N, in fact). In contrast, the design of signals with low ISL levels (high MF values), and thus good aperiodic correlation properties, has proven more challenging to researchers. The need for low ISL waveforms, as opposed to CAZAC sequences, is entirely dependent on the application and directly relates to the stationarity of the scene or channel, the maximum signal delay, and the SNR. We focus herein on the design of signals with low aperiodic correlation levels.

[TABLE 1] FLOWCHART OF THE CAN ALGORITHM.

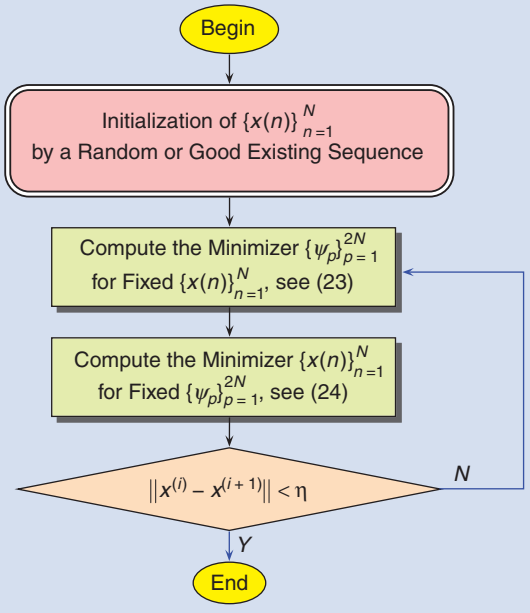

To find sequences with low autocorrelation levels that lack a closed-form expression (unlike the previous signals), researchers have used gradient descent and stochastic optimization techniques (see, e.g., [21]–[23]). These algorithms are usually computationally expensive and only perform well for small values of N, such as $N \sim 10^2$. For large values of N, a series of recently proposed cyclic algorithms (CAs) can be used to effectively minimize the ISL-related metrics locally. We outline these algorithms in the next few subsections.

THE CAN ALGORITHM

We first present a synopsis of the CA-new (CAN) algorithm proposed in [24]. Recalling the ISL definition offered in (9), and by applying the Parseval equality, the ISL of a sequence can be expressed in the frequency domain as

$$\text{ISL} = \frac{1}{2N}\sum_{p=1}^{2N}[\Phi(\theta_p) - N]^2, \tag{16}$$

where $\{\Phi(\theta_p)\}_{p=1}^{2N}$ is the DFT of $\{r(k)\}_{k=-N+1}^{N-1}$ at frequencies $\{\theta_p = 2\pi p/2N\}_{p=1}^{2N}$ [25]. Since the DFT of $\{r(k)\}_{k=-N+1}^{N-1}$ yields the spectral density function of $\{x(n)\}_{n=1}^{N}$, so that $\Phi(\theta_p) = |\sum_{n=1}^{N} x(n)e^{-j\theta_p n}|^2$, the ISL in (16) can be further expressed as

$$\text{ISL} = \frac{1}{2N}\sum_{p=1}^{2N}\left[\left|\sum_{n=1}^{N} x_n e^{-j\theta_p n}\right|^2 - N\right]^2. \tag{17}$$

Minimization of the ISL metric in (17), which is a quartic function of $\{x(n)\}_{n=1}^{N}$, can prove computationally challenging. To simplify, we instead consider the following "almost equivalent" problem [26], [24]

$$\min_{\{x(n)\}_{n=1}^{N};\{\psi_p\}_{p=1}^{2N}} \sum_{p=1}^{2N}\left|\sum_{n=1}^{N} x_n e^{-j\theta_p n} - \sqrt{N}e^{j\psi_p}\right|^2 \tag{18}$$
$$\text{s.t. } |x(n)| = 1, \quad n = 1, \ldots, N.$$

Sequences that minimize the ISL equation in (17) and those that solve the ISL-related minimization problem in (18) will, in general, be different. However, we contend that a sequence that makes the cost function in (18) small will certainly lead to a small ISL value in (17) (please see [27] for further discussion). To within a multiplicative constant, the criterion in (18) can be rewritten as

$$\|\mathbf{A}^*\mathbf{w} - \mathbf{v}\|^2, \tag{19}$$

where

$$\mathbf{w} = \left[x(1), \ \ldots, \ x(N), \ 0, \ \ldots, \ 0\right]^T_{2N\times 1}, \tag{20}$$

$$\mathbf{v} = \frac{1}{\sqrt{2}}\left[e^{j\psi_1}, \ \ldots, \ e^{j\psi_{2N}}\right]^T, \tag{21}$$

and

$$\mathbf{A}^* = \frac{1}{\sqrt{2N}}\begin{bmatrix} e^{-j\theta_1} & \cdots & e^{-j2N\theta_1} \\ \vdots & \ddots & \vdots \\ e^{-j\theta_{2N}} & \cdots & e^{-j2N\theta_{2N}} \end{bmatrix}. \tag{22}$$

If $\mathbf{f} = \mathbf{A}^*\mathbf{w}$ represents the Fourier transform of $\mathbf{w}$, then for fixed $\mathbf{f}$, the minimizer of (19) is given by

$$\psi_p = \arg(f(p)), \quad p = 1, \ldots, 2N. \tag{23}$$

Similarly, for a given $\mathbf{v}$, and if $\mathbf{g} = \mathbf{A}\mathbf{v}$ denotes the inverse Fourier transform of $\mathbf{v}$, then the minimizing sequence $\{x(n)\}_{n=1}^{N}$ of (19) is given by

$$x(n) = e^{j\arg(g(n))}, \quad n = 1, \ldots, N. \tag{24}$$

The steps of CAN, to provide the cyclic minimization of the ISL-related metric in (18), are summarized in Table 1 (where $\mathbf{x}^{(i)}$ denotes the sequence obtained at the ith iteration). Note that in Table 1, η is a predefined threshold, such as 10^{-3}. Due to its simple FFT operations [see (22)–(24)], CAN can be used to provide waveform synthesis on an ordinary PC for very large values of N, such as $N \sim 10^6$.

CAN (as well as periodic CAN, which is described in the section "The Periodic Correlation Case") shares a close relationship with the Gerchberg-Saxton algorithm (GSA) [28], which was originally presented in the optics literature more than 35 years ago. In Appendix A, we will review a version of GSA and explain its connection to the cyclic algorithms described in this article.

In Figure 2, we compare the merit factors of the P4, Frank, and CAN (initialized with a Frank sequence) sequences for the following lengths: $N = 3^2, 5^2, 10^2, 15^2, 20^2, 30^2, 70^2$, and 100^2 (note that each N is chosen to be a square to cater to the Frank sequence; the CAN algorithm does not have such a restriction). The results are shown using a log-log scale. The CAN sequence provides the highest merit factor for each value of N considered. When $N = 100^2$, the CAN sequence provides the largest merit factor of 1,769.05, which is several times larger than that given by the Frank sequence (which is 246.39). Although a Frank sequence was used here to initialize CAN, a similar result would have been obtained by initializing the algorithm with a P4 or Golomb sequence (since these chirp-based waveforms are closely related).

We provide the autocorrelation of a Frank sequence and CAN sequence (again initialized with a Frank sequence) for length $N = 100^2$ in Figure 3(a) and (b), respectively. In addition to its lower ISL value, the CAN sequence has a lower PSL (−57.27 dB) compared to the Frank signal (−49.94 dB).

THE CA ALGORITHM

In some cases, the maximum difference between the arrival times of the sequence of interest and of the interference is (much) smaller than the duration of the emitted signal (see, e.g., [29]–[31]). Consequently, for transmit sequence design in such instances, the interest lies in making $\{|r(k)|\}_{k=1}^{P-1}$ small, for some $P < N$, instead of trying to minimize all correlation sidelobes $\{|r(k)|\}_{k=1}^{N-1}$. The value of P is selected based on a priori knowledge about the application. In wireless communications, for example, significant channel tap coefficients can occur only up to a certain known maximum delay (P is chosen as the said delay). In this section, we briefly summarize the CA algorithm, which serves as an extension to CAN for this $P < N$ case. Further details, as well as an application of CA to multiple sequence sets, can be found in [32] and [26].

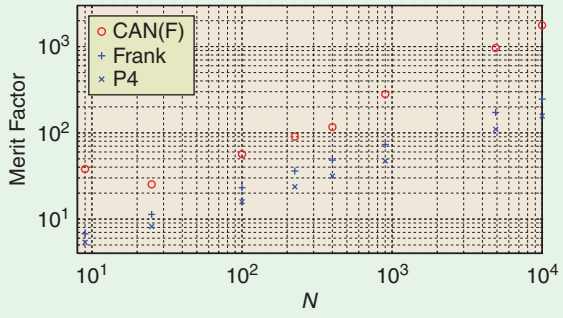

[FIG2] The merit factor versus the sequence length N for P4, Frank and CAN (initialized with a Frank sequence) sequences.

Define the following matrix:

$$\mathbf{X} = \begin{bmatrix} x(1) & & 0 \\ \vdots & \ddots & \\ \vdots & & x(1) \\ x(N) & & \vdots \\ & \ddots & \vdots \\ 0 & & x(N) \end{bmatrix}_{(N+P-1)\times P}. \tag{25}$$

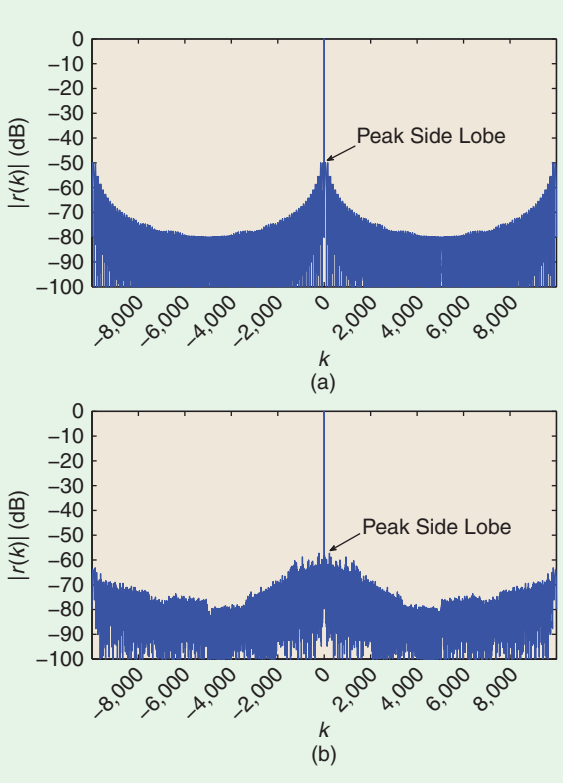

[FIG3] The autocorrelations of (a) a Frank sequence with $N = 100^2$ and (b) a CAN sequence, initialized with a Frank sequence, with $N = 100^2$.

It follows that

$$\mathbf{X}^*\mathbf{X} = \begin{bmatrix} r(0) & r(1)^* & \cdots & r^*(P-1) \\ r(1) & r(0) & \ddots & \vdots \\ \vdots & \ddots & \ddots & r^*(1) \\ r(P-1) & \cdots & r(1) & r(0) \end{bmatrix}_{P\times P}. \quad (26)$$

Minimization of the autocorrelation terms $\{|r(k)|\}_{k=1}^{P-1}$ can be achieved by minimizing the criterion $\|\mathbf{X}^*\mathbf{X} - N\mathbf{I}\|^2$. Similar to (18), we can instead define the following "almost equivalent," computationally feasible, minimization problem:

$$\min_{\{x(n)\}_{n=1}^N;\mathbf{U}} \|\mathbf{X} - \sqrt{N}\mathbf{U}\|^2 \quad (27)$$
$$\text{s.t. } \mathbf{U}^*\mathbf{U} = \mathbf{I}$$
$$|x(n)| = 1, \ n = 1, \ldots, N.$$

As in the section "The CAN Algorithm," a cyclic approach is adopted. $\mathbf{X}$ is first initialized by a randomly generated unimodular sequence. The criterion in (27) is then iteratively minimized by fixing $\mathbf{X}$ to compute $\mathbf{U}$, then fixing $\mathbf{U}$ to compute $\mathbf{X}$ (and so on, until a given stop criterion is satisfied). During this iterative process, both $\mathbf{U}$ and $\mathbf{X}$ have closed-form updating formulae (see [26] for details). Although CA does not follow an FFT-based approach, we can also extend the CAN approach described in the section "The CAN Algorithm" to design sequences whose correlation lags are only minimized over a region of interest. Further details can be found in [24].

SEQUENCE SETS

Many applications, such as MIMO radar and code division multiple access (CDMA) systems, require a set of sequences with both good auto- and cross-correlation properties. We can extend the single sequence scenario, which only considers autocorrelation, to the multiple sequence case as follows.

For a set of M unimodular sequences $\{x_m(n)\}$ ($m = 1, \ldots, M$ and $n = 1, \ldots, N$), the cross-correlation between the kth and sth sequence at time lag l is defined as

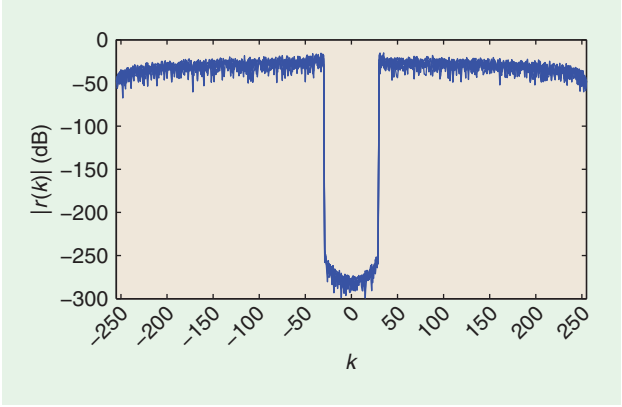

[FIG4] Overlaid cross-correlations for a CA sequence set with $M = 4$, $N = 256$, and $P = 30$.

$$r_{ks}(l) = \sum_{n=l+1}^{N} x_k(n)x_s^*(n-l) = r_{sk}^*(-l) \quad (28)$$
$$k, s = 1, \ldots, M \text{ and } \ l = 0, \ldots, N-1.$$

The ISL, which now must consider both the auto- and cross-correlations, can be extended to the multiple waveform case as

$$\text{ISL}_{\text{MIMO}} = \sum_{k=1}^{M}\sum_{l=1}^{N-1}|r_{kk}(l)|^2 + \sum_{k=1}^{M}\sum_{\substack{s=1\\ s\neq k}}^{M}\sum_{l=0}^{N-1}|r_{ks}(l)|^2. \quad (29)$$

Minimization of the ISL in (29) can be performed, for all delays, using an FFT-based approach, which allows for efficient computation and permits the design of longer sequences. This approach parallels the CAN formulation reviewed in the section "The CAN Algorithm," and we refer the reader to [27] for further details. Similarly, when the maximum lag considered is less than the sequence length, the CA approach described in the section "The CA Algorithm" can be directly applied to the multiple sequence case. More information can be found in [27], [32], and [26].

In Figure 4, we provide the cross-correlations for a set of $M = 4$ CA sequences with length $N = 256$. We consider $P = 30$ correlation lags (we are only interested in minimizing $\{r_{ks}(l)\}$ in (28) for $|l| < 30$); we overlay the set of seven cross-correlations (i.e., between the first and second waveform and the first and third waveform). As evidenced, the cross-correlations are well below -250 dB in the region of interest. The autocorrelations of the sequences (not shown) have similar, near-zero behavior in the region of interest.

THE PERIODIC CORRELATION CASE

As discussed in the section "A Review of Existing Waveforms," extensive literature exists on the design of signals with good periodic properties. Sequences having low periodic autocorrelations are useful for such applications as CDMA systems [33] and ultrasonic imaging [34]. Further, for applications involving multiple waveforms, sequence sets with good periodic auto and cross-correlations are often desirable. For example, in asynchronous CDMA systems, low periodic autocorrelation improves synchronization and low periodic cross-correlation reduces interference from other users. In this section, we briefly describe the extension of CA to the design of CAZAC sequences of arbitrary length N (referred to as periodic CAN, or PeCAN). Unlike many existing CAZAC waveforms, periodic CA sequences do not have a closed-form expression, which is certainly desirable in many covert applications (for example, covert underwater communications [31]).

We can replace the matrix $\mathbf{X}$ in (25) with

$$\mathbf{X} = \begin{bmatrix} x(1) & x(N) & \cdots & x(2) \\ x(2) & x(1) & & x(3) \\ \vdots & \vdots & & \vdots \\ x(N) & x(N-1) & \cdots & x(1) \end{bmatrix}_{N\times N}, \quad (30)$$

where each column is a shifted version of the sequence $\{x(n)\}_{n=1}^{N}$. The matrix product $\mathbf{X}^{*}\mathbf{X}$ will now include periodic correlations at all lags, and the minimization problem in (27) (and subsequent cyclic solution) follows as before. For the design of longer sequences, we can instead adopt an FFT-based approach, similar to the one used by CAN in the section "The CAN Algorithm." We refer the readers to [35] and [36] for more details on the cyclic design of sequences with good periodic properties.

We show the superimposed (periodic) autocorrelations of 50 periodic CAN sequences of length $N = 200$ in Figure 5. In our simulation, we actually generated 100 sequences using random initializations; the 50 sequences shown represent those with the lowest ISL. As shown in Figure 5, the sidelobes for each of these sequences is below -140 dB (and can be considered zero in practice).

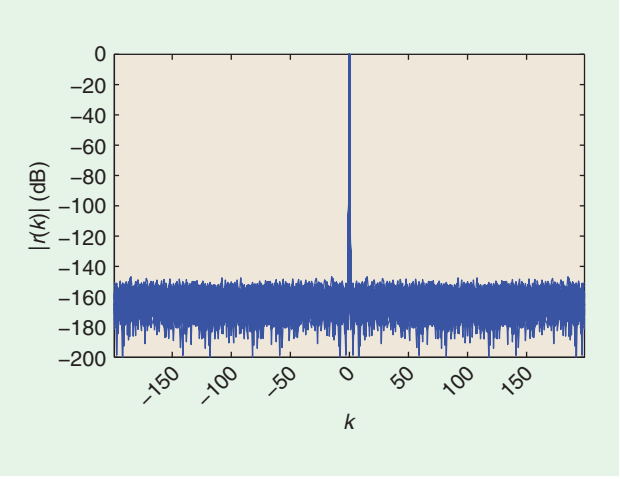

[FIG5] Overlaid autocorrelations of 50 periodic CAN sequences of length $N = 200$.

RECEIVER DESIGN

In the section "Transmit Waveform Design," we described several different waveforms, all designed to provide a high MF and thus allow for better clutter suppression at the receiver. For some cases, however, even a careful construction of the radar's transmit waveforms, when coupled with a matched filter at the receiver, still might not provide sufficient sidelobe reduction. To address these situations, we now turn our attention to the receiver stage of an active sensing system. We begin our discussion by reviewing the matched filter and by motivating the need for more advanced receiver designs.

MATCHED FILTER

A matched filter is applied, in many applications, to improve the SNR properties of the received signal (see, e.g., [12] and [37]). Ideally, a matched filter works by amplifying the signal of interest component in the received signal and by reducing the signal's noise component, which is usually assumed to be uncorrelated with the transmitted sequence(s). In the presence of stochastic additive white noise, in fact, a matched filter provides the highest SNR performance. If the transmitted waveform, or waveform set, has good correlation properties, a matched filter will also serve to weaken the reflected signals from targets in neighboring range cells to the one of interest.

After the matched filter is applied to $\mathbf{y}_{r'}$, the least-squares estimate for the reflection coefficient $\kappa_{r',l'}$ is then given by

$$\hat{\kappa}_{r',l'} = \frac{\sum_{n=1}^{N} \tilde{x}_{l'}^{*}(n) y_{r'}(n)}{\sum_{n=1}^{N} |\tilde{x}_{l'}(n)|^2} = \frac{\tilde{\mathbf{x}}_{l'}^{*} \mathbf{y}_{r'}}{\tilde{\mathbf{x}}_{l'}^{*} \tilde{\mathbf{x}}_{l'}}. \tag{31}$$

Similar estimates can be generated for the other targets in the scene by reformulating the model for the received signal in (3) (so that $\mathbf{y}_{r'}$ is aligned with the return from a range bin of interest r' for $r' = 1, \ldots, R$).

If there were no interference terms in (3) (i.e., if $\kappa_{r,l} = 0$ for any $\{r, l\} \neq \{r', l'\}$), then the matched filter would provide a highly accurate estimate of $\kappa_{r',l'}$. When interference terms (clutter) are present in the received signal, which is commonly the case in practice, then the performance of the matched filter for estimation will depend directly on the correlation properties of the transmitted sequence(s). In the section "Transmit Waveform Design," we described several cyclic approaches that can be used to design sequences (or sequence sets) with low correlations. When the correlation region of interest is small enough, as exemplified in Figure 4, we are often able to synthesize sequences (or sequence sets) with nearly zero sidelobes over the region of interest. When we wish to minimize the correlation across all sequence lags, or when Doppler effects are nonnegligible, however, it is not possible to design waveforms (or waveform sets) with zero ISL.

The autocorrelation of a waveform $s(t)$ represents the matched filter's temporal response to a target with negligible Doppler shift (a stationary target relative to the radar). If a target is moving, we have to instead consider the ambiguity function of the signal [12]

$$|\chi(\Delta t, d)| = \left| \int_{-\infty}^{\infty} s(t) s^{*}(t + \Delta t) e^{j2\pi dt} dt \right|, \tag{32}$$

where Δt again represents the relative time delay and d represents the Doppler shift of a target. Unlike the autocorrelation, the volume (sidelobes) underneath the ambiguity function for any sequence is constrained to unity (when we normalize by the energy in the signal). In Figure 6, we show the three-dimensional representation of the ambiguity function of a CAN signal (initialized with a random sequence) with length $N = 36$ (where $t_b = \tau/N$ denotes the length of each subpulse). As we can see, the ambiguity function of the CAN waveform resembles a "thumbtack" in shape. Although a "thumbtack" form is desirable, since this shape can lead to improved Doppler resolution, the total volume underneath the function remains fixed. Since we

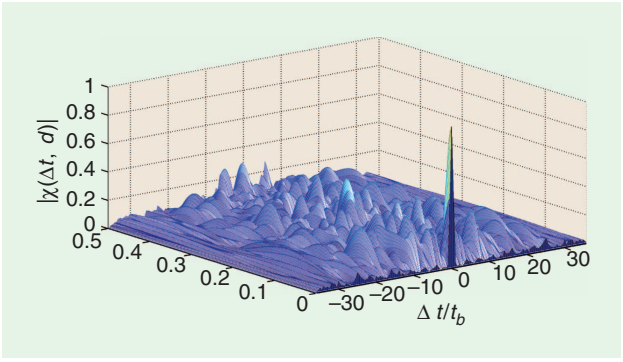

[FIG6] **Ambiguity function of a length $N = 36$ CAN function.**

are unable to design a sequence (or a set of sequences) that has zero sidelobes for all time delays and Doppler shifts in (32), we instead seek to replace the matched filter with more advanced receiver designs.

IV RECEIVE FILTER

The instrumental variables (IV) method (also called a mismatched filter), a more general approach for estimating $\kappa_{r',l'}$, can be used to significantly lower sidelobes at the cost of a reduced SNR [38], [39], [40]. Temporarily neglecting Doppler effects (so that $L = 1$, $\omega_1 = 0$, and $\widetilde{\mathbf{x}}_1 = \mathbf{x}$), the IV estimate of $\kappa_{r'}$ is given by

$$\hat{\kappa}_{r'} = \frac{\mathbf{z}^* \mathbf{y}_{r'}}{\mathbf{z}^* \mathbf{x}}, \tag{33}$$

where $\mathbf{z}$ denotes the IV receive filter. In the case $\mathbf{z} = \mathbf{x}$, then (33) reduces to the matched filter estimate of $\kappa_{r'}$. In general, and unlike the matched filter, the elements of $\mathbf{z}$ are not restricted to be unimodular, since this vector is only designed for the purposes of estimation. Also, we note that IV filters can be precomputed offline. From a computational standpoint, therefore, IV certainly offers minimal burden to the receiver, as the complexity of its application is comparable to that of the matched filter. We assume herein that $\mathbf{z}$ is a vector of length N, although, by padding the transmit waveform with zeros, a longer IV vector could be designed to improve sidelobe reduction even more (at a cost of further reduced SNR).

We consider the IV formulation given in [40]. The goal of the IV approach is to find a signal $\mathbf{z}$ that minimizes the ISL, which, in the negligible Doppler case, is given by

$$\mathrm{ISL}_{\mathrm{IV}} = \frac{\sum_{k=-(N-1),\, k\neq 0}^{N-1} |\mathbf{z}^* \mathbf{J}_k \mathbf{x}|^2}{|\mathbf{z}^* \mathbf{x}|^2}. \tag{34}$$

By applying the Cauchy-Schwartz inequality, the minimum value of $\mathrm{ISL}_{\mathrm{IV}}$ was shown to be achieved when $\mathbf{z} = \mathbf{R}_{\mathrm{IV}}^{-1}\mathbf{x}$, where

$$\mathbf{R}_{\mathrm{IV}} = \sum_{k=-N+1,\, k\neq 0}^{N-1} \mathbf{J}_k \mathbf{x}\mathbf{x}^* \mathbf{J}_k^T. \tag{35}$$

In this way, an IV receive vector, in the absence of Doppler effects, can be designed to reduce sidelobes to near zero levels. When motion is present in the scene, however, an IV filter can fail to provide satisfactory results.

We will now assume that the Doppler shifts of the targets in the scene $\{\omega_l\}_{l=1}^{L}$ are assumed to lie within an uncertainty interval denoted by $\Omega = [\omega_a, \omega_b]$ (where $\omega_b > \omega_a$ and where we choose L such that $\{\omega_l\}_{l=1}^{L}$ covers Ω). Since no knowledge is assumed of the targets' Doppler shifts, other than that they belong to Ω, the ISL criterion in (34) is rewritten as [40]

$$\mathrm{ISL}_{\mathrm{IV,\,D}} = \sum_{k=-(N-1),\, k\neq 0}^{N-1} \left(\frac{1}{\omega_b - \omega_a}\right) \frac{\int_\Omega |\mathbf{z}_{l'}^* \mathbf{J}_k \widetilde{\mathbf{x}}(\omega)|^2 d\omega}{|\mathbf{z}_{l'}^* \widetilde{\mathbf{x}}_{l'}|^2}, \tag{36}$$

where $\mathbf{z}_{l'}$ refers to the receive filter for Doppler bin l' and $\widetilde{\mathbf{x}}(\omega)$ denotes the Doppler shifted waveform (according to Doppler frequency ω). When the Doppler uncertainty interval Ω becomes larger, the minimum achievable value of $\mathrm{ISL}_{\mathrm{IV,\,D}}$ could become significantly greater than that of $\mathrm{ISL}_{\mathrm{IV}}$. Intuitively, this is due to the fact that the designs based on $\mathrm{ISL}_{\mathrm{IV,\,D}}$ are more conservative, as they try to optimize the ISL metric averaged over the entire set Ω. For this reason, the IV approach does not perform well when Doppler effects are nonnegligible.

ITERATIVE ADAPTIVE APPROACH

To provide higher resolution in the nonnegligible Doppler case, at the cost of increased computational complexity at the receiver, we now explore a more advanced estimation technique. The iterative adaptive approach (IAA), first presented in [41], was shown to offer improved resolution and interference rejection performance. IAA is a nonparametric and user parameter-free weighted least-squares algorithm. In [41], IAA was shown to perform well for applications in channel estimation, radar and sonar range-Doppler imaging, and passive array sensing. Whereas some data-adaptive algorithms require a significant number of snapshots to obtain accurate target estimates, IAA was shown to achieve good performance even with a single data vector. We briefly summarize the algorithm here.

Consider the model for $\mathbf{y}_{r'}$ in (3). The goal of IAA is to minimize the following weighted least-squares cost function with respect to a target of interest $\kappa_{r',l'}$

$$\|\mathbf{y}_{r'} - \kappa_{r',l'} \widetilde{\mathbf{x}}_{l'}\|^2_{\mathbf{Q}_{r',l'}^{-1}}, \tag{37}$$

where $\|\mathbf{u}\|^2_{\mathbf{Q}^{-1}} \triangleq \mathbf{u}^* \mathbf{Q}^{-1} \mathbf{u}$. The interference covariance matrix for a target of interest $\kappa_{r',l'}$ is denoted by $\mathbf{Q}_{r',l'}$, and is defined

$$\mathbf{Q}_{r',l'} = \mathbf{R}_{\mathrm{IAA}}(r') - |\kappa_{r',l'}|^2 \widetilde{\mathbf{x}}_{l'} \widetilde{\mathbf{x}}_{l'}^*, \tag{38}$$

where

$$\mathbf{R}_{\mathrm{IAA}}(r') = \sum_{r=-N+1}^{N-1} \sum_{l=1}^{L} |\kappa_{r'+r,l}|^2 \mathbf{J}_r \widetilde{\mathbf{x}}_l \widetilde{\mathbf{x}}_l^* \mathbf{J}_r^T. \quad (39)$$

The weighted least-squares estimate for a target of interest $\kappa_{r',l'}$, after some simplification, is given by

$$\hat{\kappa}_{r',l'} = \frac{\widetilde{\mathbf{x}}_{l'}^*(\mathbf{R}_{\mathrm{IAA}}(r'))^{-1}\mathbf{y}_{r'}}{\widetilde{\mathbf{x}}_{l'}^*(\mathbf{R}_{\mathrm{IAA}}(r'))^{-1}\widetilde{\mathbf{x}}_{l'}}, \quad l' = 1, \ldots, L, \quad r' = 1, \ldots, R. \quad (40)$$

Since the estimate in (40) depends on the covariance matrix $\mathbf{R}_{\mathrm{IAA}}(r')$, which in turn depends on the target amplitudes, the algorithm uses an iterative approach, which is summarized in Table 2. The target coefficients are initialized using the matched filter approach outlined in the section "Matched Filter." To estimate targets in other range bins, we simply redefine $\mathbf{y}_{r'}$, which represents the N length signal vector aligned with the received reflection from a range bin of interest r'. IAA typically converges after about ten iterations (which corresponds to $T_{\mathrm{IAA}} = 10$ in Table 2); a local convergence proof for IAA is offered in [42].

REGULARIZED IAA

In applications involving multiple receive antennas (which permits the use of steering beams), the angular scanning region, relative to a system's antenna array, might be reduced from the entire range (e.g., -90° to 90°) to a region of interest (e.g., -30° to 30°). Although a reduction in the size of the angular grid would certainly provide computational advantages at the receiver (fewer targets that would require an estimate), such a reduction would inevitably lead to a higher condition number for the covariance matrix $\mathbf{R}$ in (39) (and eventually threaten the invertibility of $\mathbf{R}$). To account for targets that lie outside the scanning region and to also allow for any noise in the received signal, which is not explicitly considered in (39), we might sometimes consider regularization of $\mathbf{R}$ with a diagonal matrix $\boldsymbol{\Sigma}$.

[TABLE 2] IAA FOR RANGE-DOPPLER IMAGING.

INITIALIZE $(t = 0)$

$\hat{\kappa}_{r',l'}^{(0)} = \frac{1}{N}\widetilde{\mathbf{x}}_{l'}^* \mathbf{y}_{r'}, \quad l' = 1, \ldots, L, \quad r' = 1, \ldots, R$

REPEAT $(t = t + 1)$

  FOR $r' = 1, \ldots, R$

    $\mathbf{R}_{IAA}^{(t)}(r') = \sum_{r=-N+1}^{N-1} \sum_{l=1}^{L} |\hat{\kappa}_{r'+r,l}^{(t-1)}|^2 \mathbf{J}_r \widetilde{\mathbf{x}}_l \widetilde{\mathbf{x}}_l^* \mathbf{J}_r^T$

    FOR $l' = 1, \ldots, L$

$$\hat{\kappa}_{r',l'}^{(t)} = \frac{\widetilde{\mathbf{x}}_{l'}^*(\mathbf{R}_{\mathrm{IAA}}^{(t)}(r'))^{-1}\mathbf{y}_{r'}}{\widetilde{\mathbf{x}}_{l'}^*(\mathbf{R}_{\mathrm{IAA}}^{(t)}(r'))^{-1}\widetilde{\mathbf{x}}_{l'}}$$

    END FOR

  END FOR

UNTIL $(t = T_{\mathrm{IAA}})$

An approach described as IAA-Regularized (IAA-R) was presented in [42] to automatically compute the noise powers in $\boldsymbol{\Sigma}$. In this way, IAA-R fits entirely within the user parameter-free framework of IAA. At a cost of increased computational complexity (since now the noise powers must also be computed iteratively), IAA-R was shown to outperform the original IAA for applications in MIMO radar imaging. Further details and examples can be found in [42].

NUMERICAL EXAMPLES

In this section, we will provide several numerical examples to objectively demonstrate the performance of the aforementioned approaches to transmit waveform synthesis in various active sensing applications. Further, we will seek to clarify the advantages and disadvantages of the different receive filters described in the section "Receiver Design."

ADVANCES IN COMPUTING POWER WILL CONTINUE TO HERALD NEW AND IMPROVED APPROACHES TO WAVEFORM DESIGN.

EXAMPLE 1

First, we aim to illustrate the improved estimation performance that can result by using signals (specifically the CA sequences depicted in the section "The CA Algorithm") with low autocorrelation. Consider an FIR channel impulse response with 40 randomly generated channel taps. Similar to other active sensing applications, the goal of channel estimation is to successfully determine the unknown channel taps. At the transmitter, we adopt a probing pulse of length $N = 200$. The noise in the received signal is assumed to be independent and identically distributed (i.i.d.) complex Gaussian noise with zero mean and variance given by σ^2. Using a matched filter at the receiver to estimate the channel taps, we can compare the performance of a P4 and CA transmit sequence. We assume that the length of the channel is known, so that $P = 40$ in the signal design stage.

In Figure 7, we show the mean-squared error (MSE) of the channel estimate when the noise variance σ^2 is varied from 10^{-6} to 1. We perform 500 Monte Carlo trials for each noise level. Owing to its better autocorrelation properties, the CA

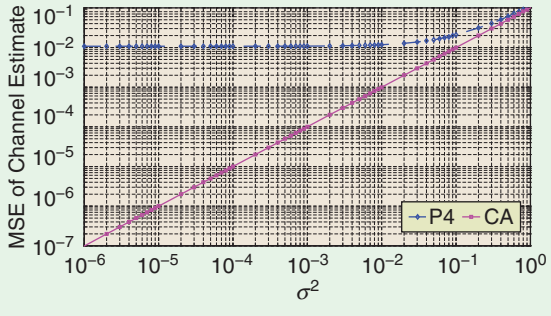

[FIG7] MSE of estimate for FIR channel with $N = 200$.

APPENDIX A

The CAN and PeCAN approaches, which were described in the sections "The CAN Algorithm" and "The Periodic Correlation Case," respectively, are closely related to the GSA that was introduced more than 35 years ago for applications in optics research (note that the cyclic approach described as GSA can also be found in an earlier paper [47], in which a proof of convergence is also provided). In this appendix, we will highlight the similarities and clarify the relationship between these waveform design algorithms and GSA.

GSA

Let $\mathbf{x}$ be an $N \times 1$ vector and consider minimizing the following criterion with respect to $\mathbf{x}$:

$$C(\mathbf{x}) = \sum_{k=1}^{K} [|\mathbf{a}_k^* \mathbf{x}| - d_k]^2, \tag{41}$$

where $d_k \in \mathbb{R}^+$ and $\mathbf{a}_k \in \mathbb{C}^{N\times 1}$ are given and K is an integer that typically satisfies $K \geq N$. In some applications, the vector $\mathbf{x}$ is free to vary in $\mathbb{C}^{N\times 1}$ (see, e.g., [48]). In other applications $\mathbf{x}$ is constrained to a certain subset of $\mathbb{C}^{N\times 1}$, such as to the set of vectors with unimodular elements. To take this fact into account, we let $\mathbf{x} \in S \subseteq \mathbb{C}^{N\times 1}$.

The GSA was introduced in [28] for tackling recovery problems typically involving a sequence and its Fourier transform. When used for problems that can be formulated as in (41), GSA has the following form:

Step 0: Given initial values $\{\psi_k^0\}_{k=1}^K$ ($\{\psi_k\}$ are auxiliary variables; see below for details), iterate Steps 1 and 2 below, for $i = 0, 1, \ldots$ until convergence.

Step 1: $\mathbf{x}^i = \arg\min_{\mathbf{x}\in S} \sum_{k=1}^{K} |\mathbf{a}_k^* \mathbf{x} - d_k e^{j\psi_k^i}|^2$. (42)

Step 2: $\psi_k^{i+1} = \arg(\mathbf{a}_k^* \mathbf{x}^i)$ and $i \leftarrow i + 1$.

The algorithm is useful when the minimization problem in Step 1 has a closed-form solution, which is obviously true for $S = \mathbb{C}^{N\times 1}$, but also for some significant instances of constraint sets (see, e.g., [24] and [35]).

Note that [28] proposed the above algorithm on heuristic grounds, without any reference to the minimization of $C(\mathbf{x})$ in (41). However, it was later shown in [49] that GSA is a minimization algorithm for (41) that has the appealing property of monotonically decreasing the criterion as the iteration proceeds. A simple proof of this fact is as follows:

$$\begin{aligned} C(\mathbf{x}^i) &= \sum_{k=1}^{K} [\,|\mathbf{a}_k^* \mathbf{x}^i| - d_k]^2 = \sum_{k=1}^{K} |\mathbf{a}_k^* \mathbf{x}^i - d_k e^{j\psi_k^{i+1}}|^2 \\ &\geq \sum_{k=1}^{K} |\mathbf{a}_k^* \mathbf{x}^{i+1} - d_k e^{j\psi_k^{i+1}}|^2 \\ &\geq \sum_{k=1}^{K} |\mathbf{a}_k^* \mathbf{x}^{i+1} - d_k e^{j\psi_k^{i+2}}|^2 = C(\mathbf{x}^{i+1}), \end{aligned} \tag{43}$$

where the first inequality is due to Step 1 and the second inequality is due to Step 2 (these inequalities are strict if the solutions computed in Steps 1 and 2 are unique, which is usually the case in applications).

The calculation in (43) provides a way to motivate GSA as a minimization algorithm for $C(\mathbf{x})$. In the following, we outline a way to derive GSA as a minimizing procedure for $C(\mathbf{x})$.

Let $\boldsymbol{\psi}$ denote a $K \times 1$ vector of auxiliary variables and let $D(\mathbf{x},\boldsymbol{\psi})$ be a function which has the property that

$$\min_{\boldsymbol{\psi}} D(\mathbf{x}, \boldsymbol{\psi}) = C(\mathbf{x}). \tag{44}$$

Then, under rather general conditions, the $\mathbf{x}$ that minimizes $C(\mathbf{x})$ is the same as the $\mathbf{x}$ obtained from the minimization of $D(\mathbf{x}, \boldsymbol{\psi})$ with respect to both $\mathbf{x}$ and $\boldsymbol{\psi}$. Evidently, for this approach to be useful the minimization of $D(\mathbf{x}, \boldsymbol{\psi})$ should be easier to handle than that of $C(\mathbf{x})$. To use the above idea in the present case of (41), we let

$$D(\mathbf{x}, \boldsymbol{\psi}) = \sum_{k=1}^{K} |\mathbf{a}_k^* \mathbf{x} - d_k e^{j\psi_k}|^2, \tag{45}$$

where $\boldsymbol{\psi}$ is the vector made from $\{\psi_k\}_{k=1}^K$. We note that the above function has the required property

transmit sequence significantly outperforms the P4 signal for smaller values of σ^2.

EXAMPLE 2

When the number of range bins in an application exceeds the length of the transmit sequence, the CAN approach (described in the section "The CAN Algorithm") can be used to generate waveforms with minimum correlation values across all lags. For this example, we will use a SISO radar system to perform range profiling of a scene. In doing so, we seek to highlight the CAN waveforms, as well as to motivate the need for better receiver design. We consider a scenario with $R = 512$ equally spaced range bins. We place three stationary (negligible Doppler effects) targets in the scene: one target at range bin 200 with amplitude -7 dB, one target at range bin 308 with amplitude -17 dB, and one target at range bin 320 with amplitude 0 dB. The transmit waveforms are designed with $N = 256$. We will assume circularly symmetric i.i.d. additive complex Gaussian noise with zero-mean and variance σ^2. The SNR, in decibels, is defined as $\text{SNR} = 10\log_{10}(1/\sigma^2)$, and is set to 20 dB. True target locations are indicated on each of the figures using an "O."

The result using a Frank sequence and a matched filter at the receiver is shown in Figure 8(a). As evidenced, the two stronger targets are successfully identified using this scheme. The third, weaker target, however, appears within the sidelobes of the strongest target, and the matched filter does not produce a peak at the true target location. In Figure 8(b), we again use a matched filter, but now transmit a CAN waveform. Since $R > N$ for this imaging example, we choose a CAN sequence, as opposed to a CA sequence, to effectively minimize all correlation lags in the waveform synthesis stage. For this case, sidelobes are reduced, and a peak is now discernible at the location of the weakest target. We use CAN waveforms for the remaining figures.

We adopt an IV receive filter (with length N) in Figure 8(c). Compared to the matched filter result in Figure 8(b),

$$\min_{\boldsymbol{\psi}} D(\mathbf{x},\boldsymbol{\psi}) = \min_{\boldsymbol{\psi}} \sum_{k=1}^{K} [|\mathbf{a}_k^* \mathbf{x}|^2 + d_k^2 - 2|\mathbf{a}_k^* \mathbf{x}| d_k \cos(\arg(\mathbf{a}_k^* \mathbf{x}) - \psi_k)]$$
$$= \sum_{k=1}^{K} [|\mathbf{a}_k^* \mathbf{x}| - d_k]^2 = C(\mathbf{x}). \quad (46)$$

The minimization of $D(\mathbf{x}, \boldsymbol{\psi})$ with respect to $\mathbf{x}$ (unconstrained as in [48] or constrained as in [24]) for fixed $\boldsymbol{\psi}$ and, respectively, with respect to $\boldsymbol{\psi}$ for fixed $\mathbf{x}$ has simple closed-form solutions. Consequently $D(\mathbf{x}, \boldsymbol{\psi})$, and hence $C(\mathbf{x})$, can be minimized conveniently via a cyclic algorithm in which $\boldsymbol{\psi}$ is fixed to its most recent value and $D(\mathbf{x}, \boldsymbol{\psi})$ is minimized with respect to $\mathbf{x}$, and vice versa. The so-obtained algorithm is nothing but the GSA in (42) and its property in (43) follows immediately from (44) and the fact that the cyclic minimization of $D(\mathbf{x}, \boldsymbol{\psi})$ yields the following monotonically decreasing sequence of criterion values: $C(\mathbf{x}^i) = D(\mathbf{x}^i, \boldsymbol{\psi}^{i+1}) \geq D(\mathbf{x}^{i+1}, \boldsymbol{\psi}^{i+2}) = C(\mathbf{x}^{i+1})$.

The general approach based on (45) can be applied to other problems for which it can lead to algorithms that have little, if anything, in common with GSA (see, e.g., [50]).

CAN AND PeCAN

The central problem dealt with in [24] and [35], as well as in the sections "The CAN Algorithm" and "The Periodic Correlation Case," was the design of a code sequence with impulse-like aperiodic and, respectively, periodic correlations. A main result proved in these papers was the fact that the said problem can be reduced to that of minimizing a criterion of the form

$$\widetilde{C}(\mathbf{x}) = \sum_{k=1}^{K} [|\mathbf{a}_k^* \mathbf{x}|^2 - d_k^2]^2, \quad (47)$$

for a certain K, $\{\mathbf{a}_k\}$, and $\{d_k\}$. In the context of the section "The CAN Algorithm" [see (17)], $K = 2N$, $\mathbf{a}_k = [e^{j\theta_k} \quad \dots \quad e^{j\theta_k N}]^T$, and $d_k = \sqrt{N}$ (where $\theta_k = 2\pi k/2N$, for $k = 1, \dots, 2N$).

The criterion in (47) might seem rather similar to $C(\mathbf{x})$ in (41), but in fact there are important differences between these two criteria. A first difference is that (44)–(46) obviously do not hold for $\widetilde{C}(\mathbf{x})$. Consequently one cannot derive a GS-type algorithm for (47) by following the approach based on (44) and (45). Of course, we could use a $\widetilde{D}(\mathbf{x}, \boldsymbol{\psi})$ defined as

$$\widetilde{D}(\mathbf{x}, \boldsymbol{\psi}) = \sum_{k=1}^{K} |(\mathbf{a}_k^* \mathbf{x})^2 - d_k^2 e^{j\psi_k}|^2 \quad (48)$$

for which it holds that $\min_{\boldsymbol{\psi}} \widetilde{D}(\mathbf{x}, \boldsymbol{\psi}) = \widetilde{C}(\mathbf{x})$, as required. However, the minimization of $\widetilde{D}(\mathbf{x}, \boldsymbol{\psi})$ is not easier than that of $\widetilde{C}(\mathbf{x})$.

To get around the above problem, a principal observation made in [24] and [35] was that, under certain conditions, the minimization of (47) is almost equivalent (in a sense specified in [35]) to that of $D(\mathbf{x}, \boldsymbol{\psi})$ in (45). Using this observation and the minimization approach outlined in the paragraph following (46), the CAN and PeCAN algorithms were introduced in [24] [35] for minimizing $D(\mathbf{x}, \boldsymbol{\psi})$ (see the sections "The CAN Algorithm" and "The Periodic Correlation Case," respectively). These algorithms have the same form as the GSA in (42). However, note that now the minimization of $D(\mathbf{x}, \boldsymbol{\psi})$ does not necessarily provide a solution to the problem of minimizing $\widetilde{C}(\mathbf{x})$. In particular, a second difference between the criteria $C(\mathbf{x})$ and $\widetilde{C}(\mathbf{x})$ is that the algorithms do not guarantee that the criterion $\widetilde{C}(\mathbf{x})$ monotonically decreases as the iteration proceeds (only $D(\mathbf{x}, \boldsymbol{\psi})$ is monotonically decreased by each iteration).

Finally, we remark on the fact that the weighted CAN and multivariate CAN algorithms (introduced in [24] and [27] and reviewed in the sections "The CA Algorithm" and "Sequence Sets," respectively), although related to GSA in their basic principles, have a weaker connection to GSA than CAN and PeCAN. These algorithms, which have been obtained by means of the "almost equivalent" minimization approach mentioned in the previous paragraph, can be viewed as extensions of GSA to problems that have more involved forms than (41) (these problems, as considered in [24] and [27], are associated with the design of sequences with more complex correlations than an impulse-like shaped one).

IV is able to further suppress sidelobe levels and to form well-separated peaks at each of the true target locations (with a negligible increase in computation). IAA (whose result is not shown) achieves similar performance to the IV filter, but at the cost of increased computational efforts at the receiver.

EXAMPLE 3

We now simulate an angle-range synthetic aperture radar (SAR) imaging example using a MIMO antenna scheme (e.g., an airborne radar that scans a ground scene with stationary targets). For this application, we will demonstrate the performance of the IAA approach for receiver design and furthermore showcase the CA sequence sets described in the section "Sequence Sets." To extend the received signal model given in (3) (as well as the receiver designs offered in the section "Receiver Design") to the MIMO case, please refer to [42] and [26]. The MIMO system under consideration contains a uniform linear array with five transmit antennas spaced at $2.5\lambda_0$ and five receive antennas spaced at $0.5\lambda_0$, where λ_0 denotes the carrier wavelength of the system. In this way, i.e., with a sparse transmit array and filled receive array, we effectively create a filled virtual array with $NM = 25$ antennas [43]–[45]. The radar collects data at five positions, with $12.5\lambda_0$ separation between each position. The ground truth consists of 16 targets, with amplitude 0 dB, placed randomly (both in angle and range) within $R = 24$ range bins. True target locations are again indicated on each of the figures using an "O," where now each symbol is colored according to its corresponding amplitude. We let the angular scanning region range from -30° to 30° with 1° grid size. We will use a CA sequence set for transmission with a length of 128. The SNR is 40 dB, where we assume i.i.d. circularly symmetric complex Gaussian noise.

We show the angle-range imaging results in Figure 9. At the receiver, we use a matched filter in Figure 9(a). To improve

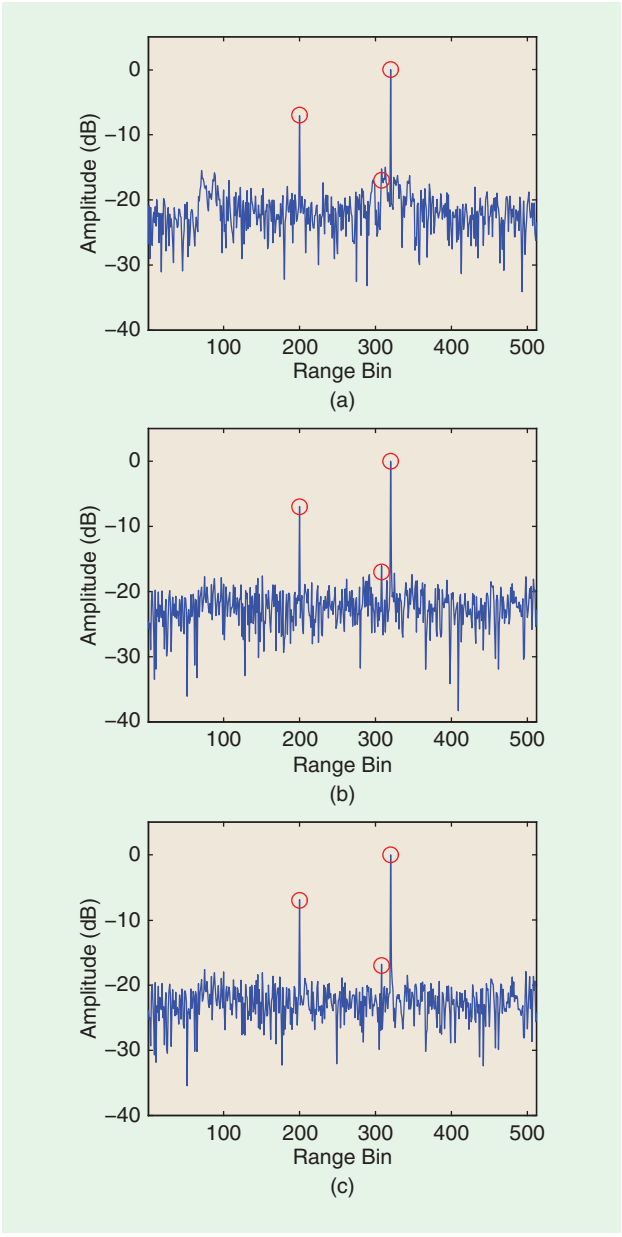

[FIG8] **Range profiles for $N = 256$, SNR = 20 dB, and using (a) a Frank sequence with a matched filter at the receiver, (b) a CAN sequence with a matched filter at the receiver, and (c) a CAN sequence with an IV receive filter. "O" denotes a true target location.**

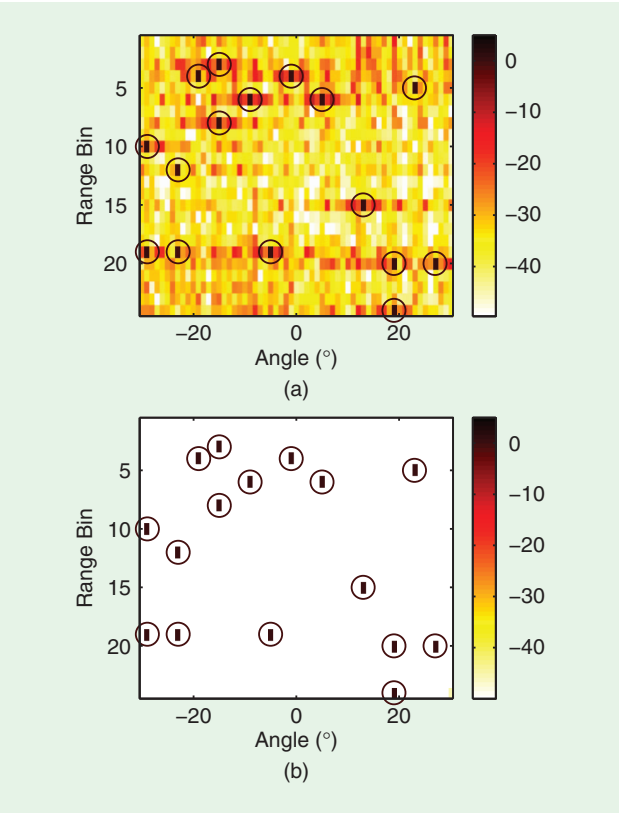

[FIG9] **MIMO angle-range images for CA transmit sequences with $N = 128$, SNR = 40 dB, and using (a) a matched filter and (b) IAA-R. Results shown are in dB. True target locations are indicated by "O."**

resolution, we apply IAA-R to the received signal in Figure 9(b). Since the scanned angular region is reduced from 180° to only cover a region of interest (for computational purposes), we apply the regularized version of IAA to account for interferences outside the scanning region. As shown, the targets are clearly identifiable using IAA-R (in fact, a perfect result is obtained).

EXAMPLE 4

Finally, we will consider range-Doppler imaging using a SISO radar system (or, equivalently for our simulation, a SISO sonar system). By incorporating an example with nonnegligible Doppler effects, we hope to demonstrate the need for the IAA algorithm addressed in the section "Iterative Adaptive Approach" (an advanced, more computationally demanding approach to receiver design). The intrapulse Doppler shift of a target is represented by $\Phi_l = \omega_t N(180^\circ/\pi)$, where $l = 1, \ldots, L$. The scene contains $R = 100$ equally spaced range bins and $L = 37$ Doppler bins with 5° separation between bins (we define Ω by setting $\Phi_1 = -90^\circ$ and $\Phi_L = 90^\circ$). We consider three targets in the scene. The first target is located at range bin 60 with Doppler shift -10° and amplitude 10 dB. The second and third targets have Doppler shift 10° and amplitude 30 dB, and are located at range bin 40 and range bin 65, respectively. The SNR is set at 10 dB (relative to a target of amplitude 0 dB and again, assuming circularly symmetric i.i.d. noise). We use a CAN transmit waveform of length $N = 36$.

The imaging result obtained using a matched filter at the receiver is shown in Figure 10(a). As shown, the matched filter fails to provide a peak at the location of the weakest target. The IV filter (whose result is omitted) shows similar performance compared to the matched filter for this nonnegligible Doppler case. The IAA result is shown in Figure 10(b). Compared to the matched and IV filters, IAA significantly reduces sidelobes and produces a peak at each of the true target locations (again, at the cost of increased computation).

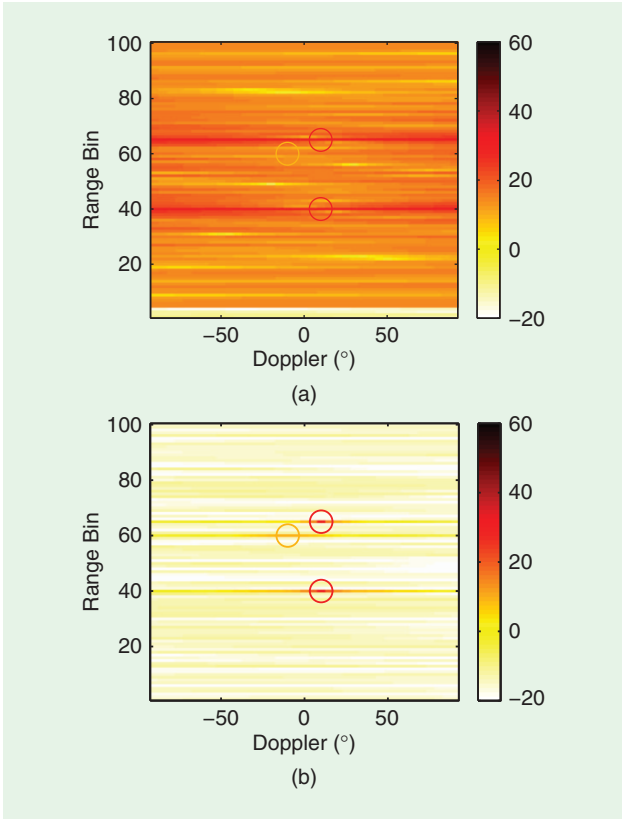

[FIG10] Range-Doppler images for a CAN transmit sequence with length $N = 36$, SNR = 10 dB, and using (a) a matched filter and (b) IAA. Results shown are in decibels.

CONCLUSIONS

For decades, researchers have sought to improve the performance of active sensing systems by designing transmission sequences with better correlation properties. Many sequences exhibit perfect periodic correlation, which is desired for some applications in communications and imaging. Other applications, including radar and sonar, demand waveforms with improved aperiodic properties. Due to the difficult computational nature of this problem, the design of sequences with good aperiodic correlation has remained an unsolved and largely evolving research field. In this article, we have provided a brief tutorial of several cyclic algorithms that can be used to efficiently generate sequences and sequence sets with superior auto- and cross-correlations. We described how this cyclic approach to waveform design can be extended to design perfect periodic waveforms. When further improvements in resolution and interference suppression are needed and cannot be met in the signal design stage, better signal processing at the receiver is required. At the expense of a loss in SNR, IV receive filters, which can be precomputed offline, can provide improved performance in the negligible Doppler (stationary target) case compared to a matched filter. When motion is present in the scene, IAA, at the cost of increased computational burden, was shown to produce higher resolution and more accurate target estimates.

Advances in computing power will continue to herald new and improved approaches to waveform design. While we have focused herein on the construction of signals with good correlation properties, this method of sequence design does not account for the Doppler properties of waveforms, which are instead represented by the well-known ambiguity function. The design of signals with specific range-Doppler characteristics is a computationally challenging and application-specific task, and will certainly remain the frontier of research in this field for years to come. In addition, with the increasing popularity of MIMO communications and MIMO radar, we can certainly expect future work to continue to focus on the design of sequence sets with good auto- and cross-correlations, a previously prohibitive (computationally) research area.

ACKNOWLEDGMENTS

This work was supported in part by the SMART Fellowship Program, the U.S. Army Research Laboratory and the U.S. Army Research Office under grant W911NF-07-1-0450, the Swedish Research Council (VR), the European Research Council (ERC), the National Science Foundation under grants CCF-0634786, ECCS-0729727, and ECS-0621879; and the Office of Naval Research under grant 00014-09-1-0211.

AUTHORS

William Roberts (WRoberts83@hotmail.com) received his B.Sc. and M.Sc. degrees in electrical and computer engineering from the University of Florida in 2006 and 2007, respectively. He is currently finishing a Ph.D. degree in the Department of Electrical and Computer Engineering at the University of Florida. His research focus includes radar signal processing and spectral estimation.

Hao He (haohe@ufl.edu) received the B.Sc. degree from the University of Science and Technology of China (USTC), Hefei, in 2007, and the M.Sc. degree from the University of Florida, Gainesville, in 2009, both in electrical engineering. He is currently pursuing a Ph.D. degree with the Department of Electrical and Computer Engineering at the University of Florida. His research interests are in the areas of radar/sonar waveform design and spectral estimation.

Jian Li (li@dsp.ufl.edu) received the M.Sc. and Ph.D. degrees in electrical engineering from The Ohio State University, Columbus, in 1987 and 1991, respectively. She is a professor with the Department of Electrical and Computer Engineering, University of Florida, Gainesville. Her current research interests include spectral estimation, statistical and array signal processing, and their applications. She is a Fellow of the IEEE and a Fellow of IET. She is a member of the Sensor Array and Multichannel Technical Committee of the IEEE Signal Processing Society. She is also a member of the editorial board of *IEEE Signal Processing Magazine* and *Digital Signal Processing*.

Petre Stoica (ps@it.uu.se) received his M.Sc. and Ph.D. degrees in automatic control from the Polytechnic Institute of Bucharest in 1972 and 1979, respectively, and an honorary degree in science from Uppsala University in 1993. He is a professor of

systems modeling in the Department of Information Technology of Uppsala University in Sweden. His research interests are biomedical signal processing, radar signal processing, wireless communications, echo cancellation, array signal processing, time series analysis, spectral analysis, and system identification. According to the Institute of Science Information, he is one of the 250 most highly cited engineering researchers in the world. He is a Fellow of IEEE. He is also a member of the Royal Swedish Academy of Engineering Sciences, an honorary member of the Romanian Academy, a Fellow of the Royal Statistical Society, and a member of the European Academy of Sciences.

REFERENCES

[1] W. H. Mow, *Sequence Design for Spread Spectrum*. Hong Kong, China: The Chinese Univ. Press, 1995.

[2] T. Helleseth and P. V. Kumar, "Sequences with low correlation," in *Handbook of Coding Theory*, V. S. Pless and W. C. Huffman, Eds. Amsterdam, The Netherlands: Elsevier, 1998, ch. 21, pp. 1765–1853.

[3] N. Levanon and E. Mozeson, *Radar Signals*. Hoboken, NJ: Wiley, 2004.

[4] S. W. Golomb and G. Gong, *Signal Design for Good Correlation: For Wireless Communication, Cryptography, and Radar*. Cambridge, U.K.: Cambridge Univ. Press, 2005.

[5] Special Issue on Waveform Agility in Radar Systems, *IEEE Signal Processing Mag.*, vol. 26, no. 1, Jan. 2009.

[6] J. J. Benedetto, I. Konstantinidis, and M. Rangaswamy, "Phase-coded waveforms and their design: The role of the ambiguity function," *IEEE Signal Processing Mag.*, vol. 26, pp. 22–31, Jan. 2009.

[7] R. Calderbank, S. D. Howard, and W. Moran, "Waveform diversity in radar signal processing," *IEEE Signal Processing Mag.*, vol. 26, pp. 32–41, Jan. 2009.

[8] J. Li and P. Stoica, "MIMO radar with colocated antennas: Review of some recent work," *IEEE Signal Processing Mag.*, vol. 24, pp. 106–114, Sept. 2007.

[9] A. H. Haimovich, R. S. Blum, and L. J. Cimini, "Mimo radar with widely separated antennas," *IEEE Signal Processing Mag.*, vol. 25, pp. 116–129, Jan. 2008.

[10] J. Li and P. Stoica, Eds. *MIMO Radar Signal Processing*. Hoboken, NJ: Wiley, 2009.

[11] D. Tse and P. Viswanath, *Fundamentals of Wireless Communication*. Cambridge, U,K.: Cambridge Univ. Press, 2005.

[12] M. I. Skolnik, *Radar Handbook*, 2nd ed. New York: McGraw-Hill, 1990.

[13] J. Jedwab, "A survey of the merit factor problem for binary sequences," in *Sequences and Their Applications—SETA 2004* (Lecture Notes in Computer Science, vol. 3486), T. Helleseth, D. Sarwate, H. Y. Song, and K. Yang, Eds. Heidelberg: Springer-Verlag, 2005, pp. 30–55.

[14] T. Høholdt, "The merit factor problem for binary sequences," in *Applied Algebra, Algebraic Algorithms and Error-Correcting Codes* (Lecture Notes in Computer Science, vol. 3857), M. Fossorier, H. Imai, S. Lin, and A. Poli, Eds. Heidelberg: Springer-Verlag, 2006, pp. 51–59.

[15] R. H. Barker, "Group synchronizing of binary digital systems," in *Communication Theory*, W. Jackson, Ed. London, U.K.: Butterworths, 1953, pp. 273–287.

[16] R. Turyn, "On Barker codes of even length," *Proc. IEEE*, vol. 51, no. 9, p. 1256, 1963.

[17] S. Eliahou and M. Kervaire, "Barker sequences and difference sets," *L'Enseignement Math.*, vol. 38, no. 2, pp. 345–382, 1992.

[18] S. W. Golomb, *Shift Register Sequences*. San Francisco, CA: Holden-Day, Inc., 1967.

[19] R. Frank, "Polyphase codes with good nonperiodic correlation properties," *IEEE Trans. Inform. Theory*, vol. 9, pp. 43–45, Jan. 1963.

[20] B. Lewis and F. Kretschmer, Jr., "Linear frequency modulation derived polyphase pulse compression codes," *IEEE Trans. Aerosp. Electron. Syst.*, vol. AES-18, pp. 637–641, Jan. 1991.

[21] M. Friese and H. Zottmann, "Polyphase Barker sequences up to length 31," *Electron. Lett.*, vol. 30, pp. 1930–1931, Nov. 1994.

[22] A. R. Brenner, "Polyphase Barker sequences up to length 45 with small alphabets," *Electron. Lett.*, vol. 34, pp. 1576–1577, Aug. 1998.

[23] P. Borwein and R. Ferguson, "Polyphase sequences with low autocorrelation," *IEEE Trans. Inform. Theory*, vol. 51, pp. 1564–1567, Apr. 2005.

[24] P. Stoica, H. He, and J. Li, "New algorithms for designing unimodular sequences with good correlation properties," *IEEE Trans. Signal Processing*, vol. 57, pp. 1415–1425, Apr. 2009.

[25] P. Stoica and R. L. Moses, *Spectral Analysis of Signals*. Englewood Cliffs, NJ: Prentice-Hall, 2005.

[26] J. Li, P. Stoica, and X. Zheng, "Signal synthesis and receiver design for MIMO radar imaging," *IEEE Trans. Signal Processing*, vol. 56, pp. 3959–3968, Aug. 2008.

[27] H. He, P. Stoica, and J. Li, "Designing unimodular sequence sets with good correlations—Including an application to MIMO radar," *IEEE Trans. Signal Processing*, vol. 57, pp. 4391–4405, Nov. 2009.

[28] R. Gerchberg and W. Saxton, "A practical algorithm for the determination of the phase from image and diffraction plane pictures," *Optik*, vol. 35, no. 2, pp. 237–246, 1972.

[29] F. Kretschmer, Jr. and K. Gerlach, "Low sidelobe radar waveforms derived from orthogonal matrices," *IEEE Trans. Aerosp. Electron. Syst.*, vol. 27, pp. 92–102, Jan. 1991.

[30] H. A. Khan, Y. Zhang, C. Ji, C. J. Stevens, D. J. Edwards, and D. O'Brien, "Optimizing polyphase sequences for orthogonal netted radar," *IEEE Signal Processing Lett.*, vol. 13, pp. 589–592, Oct. 2006.

[31] J. Ling, Y. Yardibi, X. Su, H. He, and J. Li, "Enhanced channel estimation and symbol detection for high speed MIMO underwater acoustic communications," *J. Acoust. Soc. Amer.*, vol. 125, pp. 3067–3078, May 2009.

[32] P. Stoica, J. Li, and X. Zhu, "Waveform synthesis for diversity-based transmit beampattern design," *IEEE Trans. Signal Processing*, vol. 56, pp. 2593–2598, June 2008.

[33] N. Suehiro, "A signal design without co-channel interference for approximately synchronized CDMA systems," *IEEE J. Select. Areas Commun.*, vol. 12, pp. 837–841, June 1994.

[34] V. Diaz, J. Urena, M. Mazo, J. Garcia, E. Bueno, and A. Hernandez, "Using Golay complementary sequences for multi-mode ultrasonic operation," in *Proc. IEEE 7th Int. Conf. Emerging Technologies and Factory Automation*, UPC Barcelona, Catalonia, Spain, Oct. 1999, pp. 599–604.

[35] P. Stoica, H. He, and J. Li, "On designing sequences with impulse-like periodic correlation," *IEEE Signal Processing Lett.*, vol. 16, pp. 703–706, Aug. 2009.

[36] H. He, D. Vu, P. Stoica, and J. Li, "Construction of unimodular sequence sets for periodic correlations," in *Proc. 2009 Asilomar Conf. Signals, Systems and Computers*, Pacific Grove, CA, Nov. 1–4, 2009.

[37] G. L. Turin, "An introduction to matched filters," *IRE Trans. Inform. Theory*, vol. 6, pp. 311–329, June 1960.

[38] M. H. Ackroyd and F. Ghani, "Optimum mismatched filters for sidelobe suppression," *IEEE Trans. Aerosp. Electron. Syst.*, vol. 9, pp. 214–218, Mar. 1973.

[39] S. Zoraster, "Minimum peak range sidelobe filters for binary phase-coded waveforms," *IEEE Trans. Aerosp. Electron. Syst.*, vol. 16, pp. 112–115, Jan. 1980.

[40] P. Stoica, J. Li, and M. Xue, "Transmit codes and receive filters for radar," *IEEE Signal Processing Mag.*, vol. 25, pp. 94–109, Nov. 2008.

[41] T. Yardibi, J. Li, P. Stoica, M. Xue, and A. B. Baggeroer. "Source localization and sensing: A nonparametric iterative adaptive approach based on weighted least squares," *IEEE Trans. Aerosp. Electron. Syst.*, vol. 46, no. 1, pp. 425–443, Jan. 2010.

[42] W. Roberts, P. Stoica, J. Li, T. Yardibi, and F. Sadjadi, "Iterative adaptive approaches to MIMO radar imaging," *IEEE J. Select. Topics Signal Processing* (Special Issue on MIMO Radar and Its Applications), vol. 4, no. 1, pp. 5–20, Feb. 2010.

[43] K. Forsythe, D. Bliss, and G. Fawcett, "Multiple-input multiple-output (MIMO) radar: Performance issues," in *Proc. 38th Asilomar Conf. Signals, Systems and Computers*, Pacific Grove, CA, vol. 1, pp. 310–315, Nov. 2004.

[44] D. W. Bliss and K. W. Forsythe, "Multiple-input multiple-output (MIMO) radar and imaging: Degrees of freedom and resolution," in *Proc. 37th Asilomar Conf. Signals, Systems and Computers*, Pacific Grove, CA, vol. 1, pp. 54–59, Nov. 2003.

[45] J. Li, P. Stoica, L. Xu, and W. Roberts, "On parameter identifiability of MIMO radar," *IEEE Signal Processing Lett.*, vol. 14, pp. 968–971, Dec. 2007.

[46] W. Roberts, H. He, X. Tan, M. Xue, D. Vu, J. Li, and P. Stoica, "Probing waveform synthesis and receive filter design for active sensing systems," in *Proc. SPIE Defense, Security and Sensing Conf.*, Orlando, FL, Apr. 2009, pp. 73350H.1–73350H.13.

[47] S. M. Sussman, "Least-square synthesis of radar ambiguity functions," *IRE Trans. Inform. Theory*, vol. 8, pp. 246–254, Apr. 1962.

[48] A. Weiss and J. Picard, "Maximum-likelihood position estimation of network nodes using range measurements," *IET Signal Processing*, vol. 2, no. 4, pp. 394–404, 2008.

[49] J. R. Fienup, "Phase retrieval algorithms: A comparison," *Appl. Opt.*, vol. 21, pp. 2758–2769, Feb. 1982.

[50] H. He, P. Stoica, and J. Li. (2010, June). "Waveform design with stopband and correlation constraints for cognitive radar," in *Proc. 2nd Int. Workshop Cognitive Information Processing*. Elba Island, Italy [Online]. Available: http://plaza.ufl.edu/haohe/papers/SCAN.pdf [SP]